Energy and charge distribution of Si ions in EUV ablation plasma

Nozomi Tanaka*[a], Ryo Deguchi[a], Nao Wada[a], Hiroaki Nishimura[b]
[a]Institute of Laser Engineering, Osaka University, Yamadaoka 2-6, Suita, Osaka, Japan 565-0871;
[b]Faculty of Engineering, Fukui University of Technology, Gakuen 3-6-1, Fukui, Fukui, Japan 910-8505

ABSTRACT

Recent developments on high-power compact extreme ultraviolet (EUV or XUV) sources have enabled us to study the materials ablation induced by the irradiation of intense EUV light. The interactions of EUV light with matters along the ablation have potential advantage for the use in advanced materials processing. We have studied the charge states and their energy distributions in the EUV ablation plasma using an E×B mass-charge analyzer. The measurement was also conducted for conventional laser ablation plasma induced by a 1064 nm Nd:YAG laser. The results showed noticeable difference between EUV and laser ablations, where EUV ablation only showed singly charged Si ions, and laser ablation showed multiply charged ions up to Si^{3+}. The energy spectra of multiply charged ions were distributed in higher energy range. It has been predicted that EUV ablation plasma have higher electron density close to the solid density and lower electron temperature at 1 to few eV, while laser ablation plasma generally has lower electron density around the critical density and higher electron temperature exceeding 10 eV mainly by inverse bremsstrahlung absorption at an irradiation intensity around 10^9 W/cm^2 range. Thus, ionization did not proceed much and only singly charged ions were detected for EUV ablation and the electron impact ionization proceeded to have multiply charged ions for laser ablation. This study showed that the experimental results reflected the general characteristics of the ablation plasma, and showed possibilities of modeling of entire EUV ablation dynamics from expanding ions.

Keywords: Extreme ultraviolet, Ablation plasma expansion

1. INTRODUCTION

Recent developments of extreme ultraviolet (EUV or XUV) sources for lithography technology enabled us to seek for further advanced materials processing using intense EUV radiations. The interaction of the lights in EUV wavelength region and matter is expected to be completely different from that of lights or lasers with longer wavelength, ranging from ultraviolet to infrared. Unlike well-known inverse-bremsstrahlung photo absorption, the photon energy of EUV light is directly absorbed by the orbital electrons. The critical density for the EUV wavelength range exceeds even solid density $>10^{23}$ cm^{-3}, so that the light is not absorbed in the ablation plasma even with a nanosecond pulse. As a consequent of the photon absorption and heating mechanism, the EUV induced ablation plasma is expected to be low temperature and high density compared to the ordinal laser ablation at the same irradiation condition. Further, one of the possible applications of such intense EUV light in materials processing is utilization of the expanding particles from the ablation plasma. For example, pulsed laser deposition (PLD) is a well know laser thin film deposition method that utilizes expanding particles from ablation plasma. EUV ablation would expand possibilities new parameters and materials to process. Thus, understandings of the mechanism of materials ablation by intense EUV radiation is important issue. However, to date, not so many studies on EUV-matter interaction have been conducted [1-3]. One of the approaches to study the EUV ablation is to investigate the particles expanding from the ablation plasma, because they preserve information of the ablation plasma itself and comparably easy to measure. The aim of this study is to understand the characteristics of expanding ions from EUV ablation plasma, and EUV plasma itself by analyzing the charge distribution and each energy spectrum. The results were compared with ordinal laser ablation to clarify noticeable difference between EUV and laser ablations.

International Conference on X-Ray Lasers 2020, edited by Davide Bleiner,
Proc. of SPIE Vol. 11886, 118860S · © 2021 SPIE · CCC code:
0277-786X/21/$21 · doi: 10.1117/12.2591978

2. EXPERIMENTS

2.1 Laser produced xenon plasma EUV source

A laser produced plasma (LPP) EUV source was used in the experiment. Figure 1 shows schematic of the EUV source. Xenon frost formed on a cryogenic target was irradiated by a Nd:YAG laser with the wavelength of 1064 nm, the pulse width of 10 ns, the intensity of 10^{11}-10^{12} W/cm^2 and the repetition rate of 10 Hz. The cryogenic target consists of a cupper drum with a hollow inside and motor to rotate the drum. Liquid nitrogen introduced inside cupper drum keeps the drum surface below the melting temperature of xenon at -111.8 ◦C. The rotation speed and Xe flow rate was optimized at 191 Hz and 100 sccm to provide fresh Xe frost surface. The EUV radiation emitted from the Xe plasma was focused onto a solid Si wafer (P-type (111)) target by an ellipsoidal EUV focusing mirror. The ellipsoidal EUV mirror surface was coated with Au to maximize the total reflection and the imaging magnification was 1:1. The target irradiation angle was 45◦. The EUV emission was incoherent and non-monochromatic to maximize the EUV photons delivered at the target position. The EUV energy at the target was 13 mJ and intensity was 10^9 W/cm^{-3}. Other parameters were synchronized with the drive laser, the pulse width of 10 ns and repetition rate of 10 Hz. The wavelength ranges 9-25 nm with a peak around 11.5 nm, which covers the strong L shell photo-absorption edge of silicon at 12.49 nm. Thomson parabola mass-charge analyzer.

2.2 Thomson parabola mass-charge analyzer

The Si ion spectra was measured by a Thomson parabola mass-charge analyzer. Measurements for Nd:YAG laser (1064 nm) ablation was also conducted for comparison. The irradiation parameters were set as same as the EUV irradiation, the pulse width of 10 ns, repetition rate of 10 Hz, and intensity of 10^9 W/cm^{-3}. Figure 2 shows schematic of the Thomson parabola analyzer. It consists of an entrance aperture, a pair of magnets, a pair of electrodes, and a micro-channel plate (MCP). The detection distance and angle from the Si sample were 75 cm and 0◦ from the sample normal. The ions expanding from the Si sample were collimated at the entrance aperture. Then the ion beam entered the magnetic field and electric filed to be separated with the parabolic energy spectrum for each mass and charge ratio. The detection unit consists of an MCP, a phosphor screen, and a CCD camera. The phosphor screen projects the parabolic spectrum image of the electrons magnified by each MCP channel, then finally detected by the CCD camera as an image. Each point of the spectrum tracing is the result of displacement of ions due to the fields. Therefore, these tracings enable us to fit and calculate the corresponding kinetic energy and charge state of ions. The multiplication factor of MCP were calibrated using a reference [4]. The vacuum pressure in the EUV source during the EUV ablation shots was in the order of 10^{-1} Pa, whereas for laser ablation shots was 10^{-2} Pa, and that of Thomson parabola analyzer was 10^{-4} Pa.

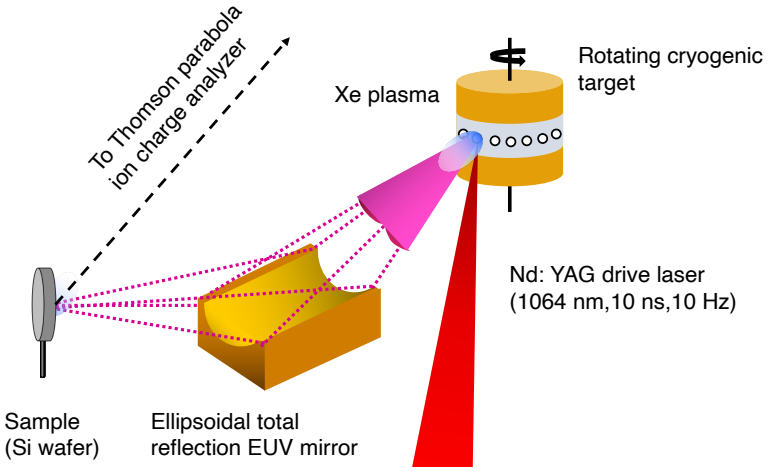

Figure 1. The laser produced plasma EUV source. EUV emitted from the laser driven xenon plasma was collected by the ellipsoidal total reflection EUV mirror and focused onto the Si wafer sample at an angle of 45◦. The Si ions expanding from the EUV ablation plasma were detected by the Thomson parabola mass-charge analyzer installed along the Si target normal.

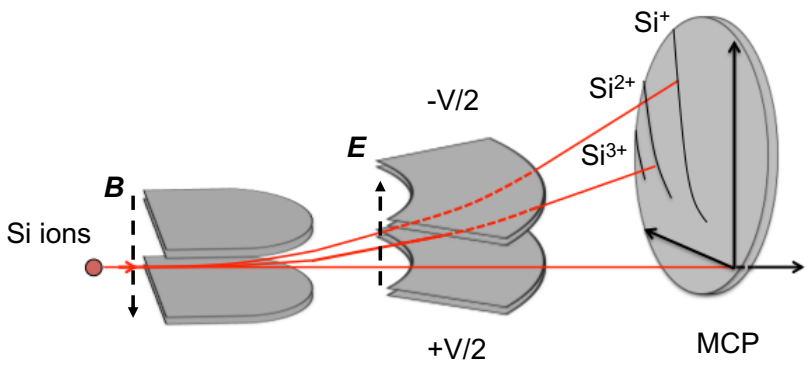

Figure 2. The Thomson parabola mass-charge analyzer. The Lorentz force applied in the magnetic field spectrally dispersed the incident ions by mass and charge ratio, then the electric field between the electrodes stretches each beam to project an energy spectrum. The energy spectra of each m/q were detected by the MCP.

3. RESULTS AND DISCUSSIONS

It is necessary to consider the influence of collision between xenon atoms and silicon ions. There are mainly two kinds of collisions, one is elastic collision and the other is inelastic collision. The inelastic collision happens when the collision energy is approximately 25 keV/u, which is equal to Bohr velocity [5]. Since this energy is far higher than the ion energy detected in our experiments, inelastic collision is negligible. Thus, we have estimated the effects of elastic collisions between Si and Xe atoms. We have estimated the elastic collision cross section of Si ion and Xe atom from that of hydrogen and Xe atoms [6-9]. The scattering cross section and velocity satisfies $\sigma \propto \upsilon^{-2/5}$ ($\upsilon \geq 6$ km/s). For example, a hydrogen atom with a velocity at 3.7×10^4 m/s, which is equivalent to 200 eV Si, gives a cross section of 6.97×10^{-15} cm^2. We have estimated element dependence on the cross section by using the effective radius of the atoms $\sigma \propto r^2$. The cross section of Si and Xe atoms were estimated as 8.6×10^{-15} cm^2 for Si atom at an energy of 200 eV. It means that 6% of Si ions arrive at the entrance aperture of the Thomson parabola analyzer that is 40 cm away from the Si sample surface in a background Xe pressure at 10^{-1} Pa. however, the reduction in numbers of particles due to the collision does not affect the ion charge state distribution at the analyzer.

Figure 3 shows ion spectra of (a) EUV ablation and (b) laser ablation. Vertical and lateral axis are attributed to magnetic and electric force respectively. The solid red lines are the fitting curves and dotted black lines are energy contour lines. Since the element detected are known as Si, the charge state can be identified from obtained parabolic tracings. The root of the black dotted lines and red solid lines is the position of zero order signal containing the neutral particles and lights, which are blocked by a physical shielding in front of the MCP. The spectra images of EUV ablation and laser ablation were completely different, where EUV ablation only showed Si^+ spectrum and laser ablation showed Si^+, Si^{2+}, and Si^{3+} spectra. Not only the charge state, but also the energy range of the spectra of laser ablation tend to be much higher. It should be noted that repulsive force among positively charged particles in ion beam, so called space charge, caused spread of each ion spectrum. The disagreement between ion spectra and fitting trace is attributed to a leakage or inhomogeneous magnetic field. Figure 4 shows the energy spectra of Si ions converted from images in fig. 3. The multiply charged ion species showed the spectrum peak at higher energy due to the charge state up to 1.2 keV of Si^{3+}. The noticeable difference between EUV and laser ablations can be qualitatively explained by the difference in ablation plasma parameters. In our previous study on expanding geometry of ions, we have simulated the plasma parameters for EUV and laser ablations of CH target at the same irradiation parameters as this study [10]. The EUV ablation showed the electron density exceeding 10^{23} cm^{-3} and electron temperature ~1 eV near the solid surface. In such plasma, the collisional ionization by thermal electrons does not proceed much and the charge state in the plasma is suppressed. The results for laser ablation showed a strong absorption of photon energy around the critical electron density, $n_e \approx 10^{21}$ cm^{-3} region. The electron temperature at the critical density region exceeded 10 eV. In general, multiply charged ions are produced via electron collisions, it is qualitatively consistent with the experimental results that only laser ablation had highly charged ions in the expanding plume. Since EUV photon absorption strongly depends on the elements due to the photon-atom atomic process, simulation of the plasma parameters for Si samples, as well as time and spatial evolutions would depict the whole dynamics of EUV ablation.

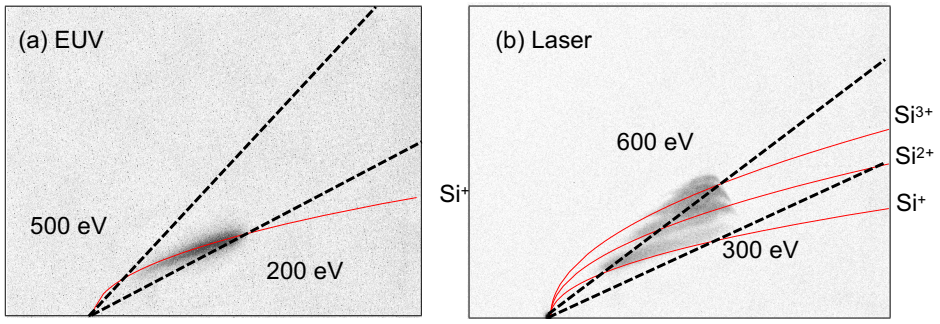

Figure 3. Ion spectra of mass-charge analysis for Si ions from (a) EUV ablation and (b) laser ablation plasmas. The solid red lines are the fitting curves and dotted black lines are energy contour lines.

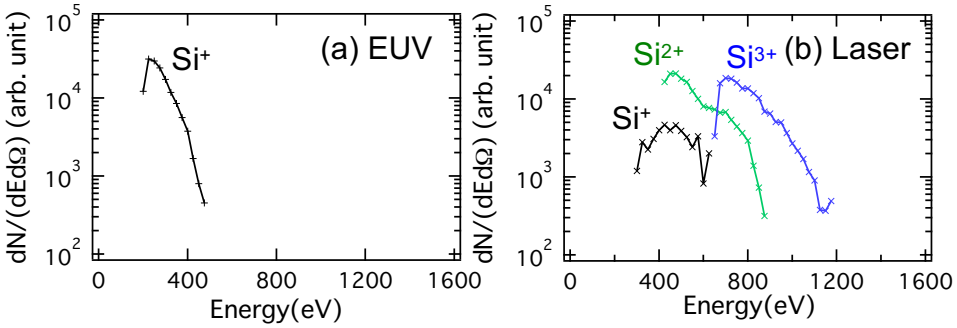

Figure 4. Energy spectra of Si ions from (a) EUV ablation and (b) laser ablation plasmas plotted from the fitting lines in fig. 3.

4. CONCLUSION

We have studied characteristics of the ions in the expanding ablation plasma, and compared EUV and laser ablations. The kinetic energy spectra of expanding ions at each charge state was obtained by a mass-charge analyzer. The results showed noticeable difference between EUV and laser ablations, where EUV ablation only showed singly charged Si ions and laser ablation showed multiply charged ions up to Si^{3+}. The energy spectra of multiply charged ions were distributed in higher energy range. The results were discussed qualitatively considering our previous simulation results on ablation plasma parameters for EUV and laser ablations. One hand, EUV ablation plasma has electron density exceeding 10^{23} cm^{-3} and electron temperature ~1 eV. Thus, ionization does not proceed much and only singly charged ions were detected. On the other hand, since laser ablation plasma tends to have lower electron density at $n_e \approx 10^{21}$ cm^{-3} and higher electron temperature T_e>10 eV, the electron impact ionization proceeds to have multiply charged ions in the signal. This study suggests that the ablation plasma characteristics and ablation mechanism can be traced back from the information of expanding ions. Further investigation with simulation studies would clarify those physics and critical difference of EUV ablation with conventional laser ablation.

ACKNOWLEDGMENT

This work was supported by JSPS Grant-in-Aid for Young Scientists (B) No. 25800303, Grant-in-Aid for Scientific Research (B) No.22340172, and MEXT Project for Creation of Research Platforms and Sharing of Advanced Research Infrastructure opening up a new photonics industry through high intensity lasers.

REFERENCES

[1] Dinh, T., Medvedev, N., Ishino, M. et al., "Controlled strong excitation of silicon as a step towards processing materials at sub-nanometer precision" Commun Phys 2, 150 (2019).

[2] G. J. Tallents, S. A. Wilson, J. Lolley, et al., "Extreme ultraviolet laser ablation of solid targets", Proc. SPIE 11111, X-Ray Lasers and Coherent X-Ray Sources: Development and Applications XIII, 1111106 (2019).

[3] H. Bravo et al., "Demonstration of Nanomachining with Focused Extreme Ultraviolet Laser Beams," in IEEE Journal of Selected Topics in Quantum Electronics 18, 443-448 (2012)

[4] B. L. Peko, and T. M. Stephen, "Absolute detection efficiencies of low energy H, H^-, H^+, H^+_2 and H^+_3 incident on a multichannel plate detector", Nucl. Instr. and Meth. in Phys. Res. B 171, 597-604 (2000).

[5] H.S.W. Massey, "Collisions between atoms and molecules at ordinary temperatures", Rep. Prog. Phys. 12, 248-269 (1949).

[6] V. Aquilanti, G. Liuti, F. Pirani, F. Vecchiocattivi, and G. G. Volpi, "Absolute total elastic cross sections for collisions of oxygen atoms with the rare gases at thermal energies", J. Chem. Phys. 65, 4751-4755 (1976).

[7] V. Aquilanti, G. Liuti, F. Vecchio„ÉªCattivi and G. G. Volpi, "Absolute total cross sections for scattering of hydrogen atoms by argon, krypton and xenon" Chem. Phys. 15, 305-308 (1972).

[8] W. C. Stwalley, A. Niehaus, and D. R. Herschbach "Hydrogen-atom scattering: Velocity dependence of total collision cross sections for rare gases and molecular hydrogen", J. Chem. Phys. 51, 2287-2288 (1969).

[9] R. B. Berstein and R. A. Labudde, "On the analysis of glory scattering data for the extraction of information on the interatomic potential well" J. Chem. Phys. 58, 1109-1117 (1973).

[10] N. Tanaka, M. Masuda, R. Deguchi, M. Murakami, A. Sunahara, S. Fujioka, A. Yogo, H. Nishimura, "Characterization of material ablation driven by laser generated intense extreme ultraviolet light" Appl. Phys. Lett. 107, 114101 (2015)

[11]. Bleiner, The Science and Technology of X-ray Lasers: A 2020 Update Proc. SPIE 11886, 1188602 (2021)